

Application of the parabolic equation method to medical ultrasonics [☆]

P. Roux^{a,*}, H.C. Song^b, M.B. Porter^c, W.A. Kuperman^b

^a *Laboratoire Ondes et Acoustique ESPCI, Université Paris VII, URA CNRS 1503, 75005 Paris, France*

^b *Marine Physical Laboratory, Scripps Institution of Oceanography, University of California, La Jolla, San Diego, CA 92093-0701, USA*

^c *Department of Mathematics, New Jersey Institute of Technology, Newark, NJ 07102, USA*

Received 31 March 1999; received in revised form 4 August 1999

Abstract

The application of the parabolic equation (PE) method is extended to hyperthermia and imaging problems in medical ultrasonics. It is shown that the PE provides an accurate solution of the acoustic field generated by a pre-focused array through an inhomogeneous medium. To investigate hyperthermia therapy, the PE is coupled with the heat equation. Simulations provide evidence that this interaction defocuses the acoustic field and degrades the efficiency of the hyperthermia treatment. We propose a procedure to maintain the focus in the zone of interest using two arrays and phase-conjugation invariance properties. For medical imaging, an algorithm is developed to move the focal spot of a linear array in any direction using a frequency shift in a time-reversal mirror (TRM). Simulations demonstrate that the proposed algorithm can be applied to an inhomogeneous medium in the presence of an aberrating layer without the knowledge of the medium properties. ©2000 Elsevier Science B.V. All rights reserved.

1. Introduction

The parabolic equation (PE) method was originally applied to model radio wave propagation in the atmosphere in the 1940s [1]. A period of extensive development began in the 1970s, when this approach was first applied to problems in ocean acoustics [2] and seismology [3]. The parabolic equation method has subsequently been applied to many types of wave propagation problems. In this paper, we apply the parabolic equation method to hyperthermia and imaging problems in medical ultrasonics.

To investigate acoustic–heat interactions in hyperthermia therapy, we solve coupled wave and heat equations. By simultaneously modeling the propagation of acoustic waves and the diffusion of heat, we are able to quantitatively simulate acoustic refraction induced by heat in the treatment volume. The interest of the PE formulation lies in the fact that one obtains the same accuracy as classical finite-difference simulation [4] in a fraction of the run-time.

[☆] Sponsored by DARPA.

* Corresponding author.

E-mail address: philippe.roux@espci.fr (P. Roux).

¹ Work done while at the Marine Physical Laboratory.

For acoustic imaging in medical ultrasonics, a time-reversal mirror (TRM) was studied extensively in the 1990s, which refocuses an incident acoustic field back to the original probe source (PS) or scatterer [5]. In this paper, we propose an algorithm to move the focal spot in any direction using a frequency shift in the presence of an aberrating layer.

This paper is divided into three parts. Section 2 reviews the efficiency and flexibility of the PE algorithm with the example of the ultrasonic field sent from a pre-focused array. Sections 3 and 4 describe the application of the PE approach to hyperthermia and medical imaging, respectively.

2. Application to ultrasonics

In this section, we summarize the structure of the most efficient PE algorithm that has been developed [6] and show its accuracy and flexibility in a classical ultrasonic configuration.

Assuming that outgoing energy dominates backscattered energy, the Helmholtz equation factors into the parabolic equation

$$\frac{\partial p}{\partial r} = ik_0 \left(\sqrt{1+X} \right) p, \quad (1)$$

where $X \equiv k_0^{-2}(\partial^2/\partial z^2 + k^2 - k_0^2)$ and $k_0 = \omega/c_0$ is a reference wavenumber. Solving this equation means that we find the pressure field $p(r + \Delta r, z)$ at the new range step using the pressure field $p(r, z)$ at the previous range step. Thus the acoustic field is obtained by a simple marching process rather than by solving a global system of equations. Range dependence is handled by approximating the medium as a sequence of range-independent regions [7].

The solution of the first-order differential equation (1) is

$$p(r + \Delta r, z) = \exp\left(ik_0\Delta r(1+X)^{1/2}\right) p(r, z), \quad (2)$$

where Δr is the range step. Applying an N -term rational function to approximate the exponential function using Padé approximations [8], we obtain

$$p(r + \Delta r, z) = \exp(ik_0\Delta r) \prod_{j=1}^N \frac{1 + \alpha_{j,N}X}{1 + \beta_{j,N}X} p(r, z), \quad (3)$$

where $\alpha_{j,N}$ and $\beta_{j,N}$, $j = 1, \dots, N$ are the complex N th-order Padé coefficients. Each Padé coefficient depends on N , the frequency ω , and the range step Δr . Based on Eq. (3), the PE algorithm is structured as follows:

1. Given the physical problem, choose a range step Δr and the order of the Padé approximation N .
2. Calculate the Padé coefficients $\alpha_{j,N}$ and $\beta_{j,N}$.
3. Given the initial pressure field $p(r_0, z)$, use the Padé approximation of Eq. (3) to successively calculate the pressure field $p(r_0 + n\Delta r, z)$, where n is a positive integer.

To check the accuracy of the PE algorithm in the ultrasonic application, we compute the pressure field in the focal plane of an ultrasonic 1-D pre-focused array and compare it to the theoretical solution in Fig. 1. Here the acoustic frequency is 1.5 MHz, the array aperture is 50 mm and the focal distance is 50 mm. For a range step $\Delta r = 1$ mm, note that the PE solution is closer to the theoretical solution with an $N = 3$ Padé approximation. As expected, the accuracy of the PE solution depends on the order of the Padé approximation. In general, the higher the order of the Padé approximation, the better the PE solution at wide angles. Moreover, we see in Fig. 1(b) that the order of the Padé approximation has to be increased for a larger Δr to get an accurate solution. In our example, for range steps of $\Delta r = 1, 5$ and 10 mm, the PE simulation converges to the theoretical solution for $N = 3, 5$ and 8, respectively. Of course, this depends on the details of the test case so that N has to be adjusted to Δr for each particular physical problem.

The efficiency of the PE algorithm can be improved by a variable range step. For example, suppose that we want to map very precisely the pressure field in a 20 mm square around the $F = 50$ mm focal point of the pre-focused

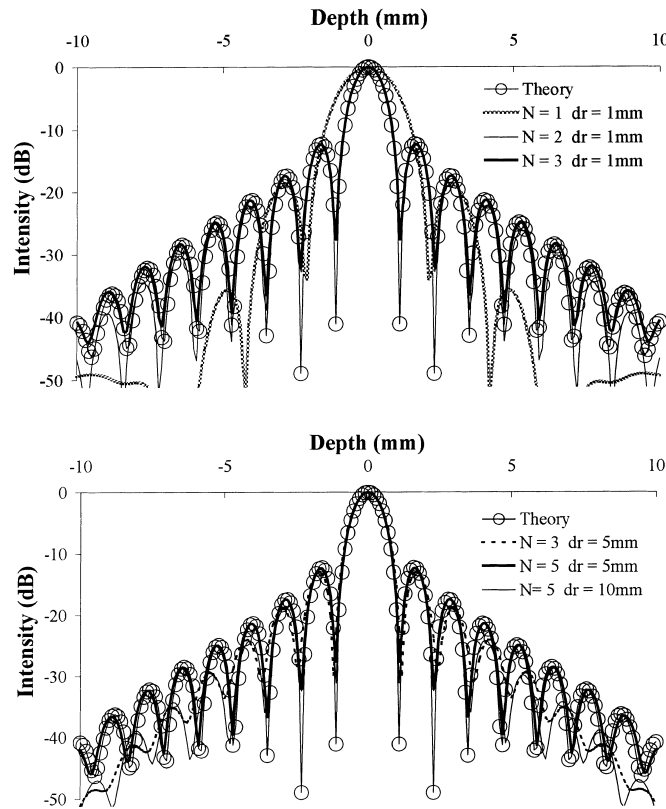


Fig. 1. Comparison of the theoretical solution and the PE numerical solution of the pressure field at the focus of an ultrasonic array. The PE algorithm is defined by an order of Padé approximation N and a range step Δr .

ultrasonic array. To do so, we need a small grid size $\Delta r = \Delta z = 0.1$ mm around the focal point. If we are to use this Δr from the array ($r = 0$) up to the focal point ($F = 50$ mm), the algorithm becomes very time consuming. However, the PE approach permits an easy two-stage procedure as shown in Fig. 2. In the first stage, we compute the field from $r = 0$ to $r = 40$ mm with an $N = 8$, $\Delta r = 10$ mm Padé approximation. In the second stage, we compute the field in the zone of interest between $r = 40$ and $r = 60$ mm using $N = 2$, $\Delta r = 0.1$ mm Padé approximation. In the next two sections, we apply the PE algorithm to hyperthermia and imaging problems in medical ultrasonics.

3. Accurate hyperthermia therapy using two ultrasonic arrays

One of the advantages of ultrasound phased-array treatments is the non-invasive manner in which ultrasonic energy and thereby heat, can be delivered to the treatment volume. However, the heat generated in the medium induces variations in the sound speed, that affect the acoustic focusing and leads to strong effects such as self-focusing or self-defocusing of the sound beam.

In order to investigate the heat–ultrasound interactions in tissue, a non-linear formulation is introduced by coupling the wave and heat equations. This formulation allows for change in the acoustic sound speed due to acoustic heating. More precisely, by assuming the acoustic streaming effect is negligible compared to acoustic heating, we obtain the coupled Eqs. (4)–(6),

$$\frac{\partial p}{\partial r} = ik_0 \left(\sqrt{n^2 + \frac{1}{k_0^2} \frac{\partial^2}{\partial z^2}} \right) p, \tag{4}$$

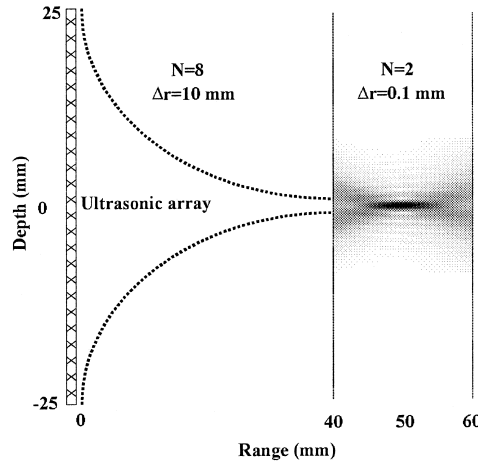


Fig. 2. Flexibility of the PE algorithm: pressure field is computed from one plane to another using different range step Δr and different order of Padé approximation N .

$$\frac{\partial T}{\partial t} = \kappa \Delta T + \frac{2\alpha I}{\rho c_t}, \quad (5)$$

$$n = \frac{c_0}{c(r, z)} = f(T(r, z)). \quad (6)$$

Eq. (4) is equivalent to Eq. (1). Eq. (5) is the so-called bio-heat transfer equation (BHTE) [9], a descriptive model which approximates the thermal characteristics of tissue. Here $T = T(r, z, t)$ is the tissue temperature, κ the heat diffusion coefficient, α the absorption coefficient of tissue, ρ the density, and c_t is the thermal capacity. $I = I(r, z, \omega)$ is the acoustic intensity which is related to the pressure by $I = |p|^2/2(\rho c)$. The acoustic intensity I is primarily attenuated by absorption mechanisms that generate heat Q in the tissue such that $Q = 2\alpha I$ as shown on the right side of Eq. (5). Note that heat is also carried away by blood leading to the so-called perfusion term [10], which is not included here for simplicity. Finally, Eq. (6) takes into account the dependence of sound speed on temperature, which will be discussed shortly.

To solve this set of coupled equations, we first compare the characteristic timescale of Eqs. (4) and (5). In our simulation, the acoustic frequency of $f = 1.5$ MHz which corresponds to a wavelength of $\lambda = 1$ mm and a characteristic timescale $1/f \sim 10^{-6}$ s. The heat diffusion coefficient κ is on the order of 10^{-7} m²/s in biological tissue [11]. Thus the dynamic timescale Δt of Eq. (5), representing the time interval after which the temperature has spread over one wavelength λ due to heat diffusion, is $\Delta t \approx \lambda^2/\kappa \approx 10$ s. Since $\Delta t \gg 1/f$, then it follows that the heterogeneity of sound speed due to heat in the medium described by Eq. (6) is a slowly dependent function of time and space.

In this case the acoustic heating can be considered as a steady state temperature field with respect to the rapidly oscillating sound field. Thus, the heat equation and the acoustic equation (in the PE approximation) can be treated separately: first, the solution of the PE gives the heat source term that is injected into the heat equation. This heat equation allows us then to compute a new temperature distribution that changes the sound speed field. Next, this new sound speed distribution is injected back into the PE equation thus closing the loop. This process has been developed independently by Le Floch et al. [4], but they compute the acoustic field with a 2-D finite-difference simulation. The advantage of the PE formulation used here lies in the fact that, for the same accuracy, the PE code runs much faster.

Our simulations are carried out in two dimensions. The acoustic field is computed by the PE algorithm described above and the temperature field is calculated by a finite difference method. Fig. 3 shows a schematic of simple hyperthermia treatment. The acoustic source is a 50 mm finite-aperture array outside the treatment volume in a

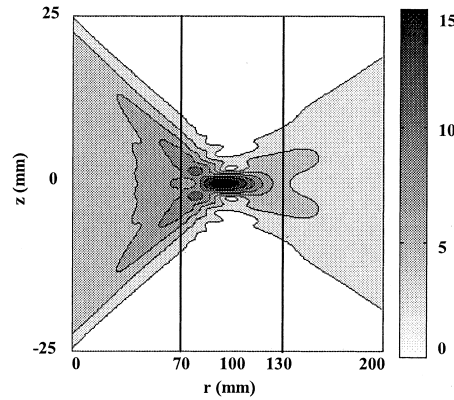


Fig. 3. Acoustic focusing with a wide-angle PE code in an absorbing medium. The solid lines delimit the treatment volume and gray level denotes the pressure in atm. The intensity at the focal point is 96.9 W/cm^2 . The size of the focal spot is 20 mm along the x -axis and 2.5 mm along the y -axis.

water bath used as a lossless coupling medium. We consider the zone of interest, between $r = 70$ and $r = 130$ mm in Fig. 3, as a fluid medium (we neglect shear waves). The density, sound speed, and temperature in this medium before treatment are taken equal to those of the coupling medium ($c = 1500 \text{ m/s}$, $\rho = 1000 \text{ kg/m}^3$). The emitted field is phased to focus at $r = 100$ mm in the zone of interest where attenuation ($\alpha = 10 \text{ N/m}$) produces heat [12]. The maximum intensity at the focus is less than 100 W/cm^2 , which means that we stay in the linear regime justifying the use of a linear PE algorithm. The duration of insonification is set at 10 s in our simulations.

Note that the pressure level at the focus is about 15 atm. Even outside of the focal point, the acoustic pressure exceeds the ambient pressure (1 atm), which violates the small signal assumption in linear acoustics. In hyperthermia, however, the nonlinearity resulting from high intensity is generally suppressed by the strong absorption in biological tissue. To measure the significance of non-linearity over the attenuation, the Goldberg number G is introduced, which is defined by l_a/l_s , where l_a and l_s are the absorption length and shock distance [13,14]. When G is small, the attenuation is dominant over the nonlinearity so that the harmonics produced by nonlinearity are dissipated by the medium and most of the acoustic energy remains in the fundamental frequency, which permits the use of a linear wave equation. On the other hand, when G is large, the nonlinearity is no longer negligible. In the hyperthermia treatment, a typical value of G is about 0.1 outside of the focal point, which justifies the use of a linear PE algorithm.

Roughly speaking, hyperthermia consists of locally heating the medium at the acoustic focal point. To understand the acoustic refraction induced by heat, two cases are studied: if the sound speed increases with temperature ($\partial c/\partial T > 0$, e.g., muscle), we observe a *self-defocusing* of the acoustic field, whereas we see a *self-focusing* [13] of the acoustic beam if the sound speed decreases with temperature ($\partial c/\partial T < 0$, e.g., fat tissue). The physics behind these two cases are different because Snell’s laws induces a different refraction depending on the sign of $\partial c/\partial T$ along an acoustic ray as shown in Fig. 4.

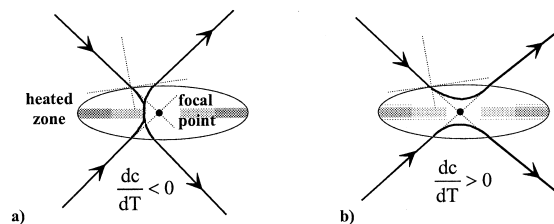


Fig. 4. (a) $\partial c/\partial T < 0$: self-focusing of the acoustic beam. (b) $\partial c/\partial T > 0$: self-defocusing of the acoustic beam.

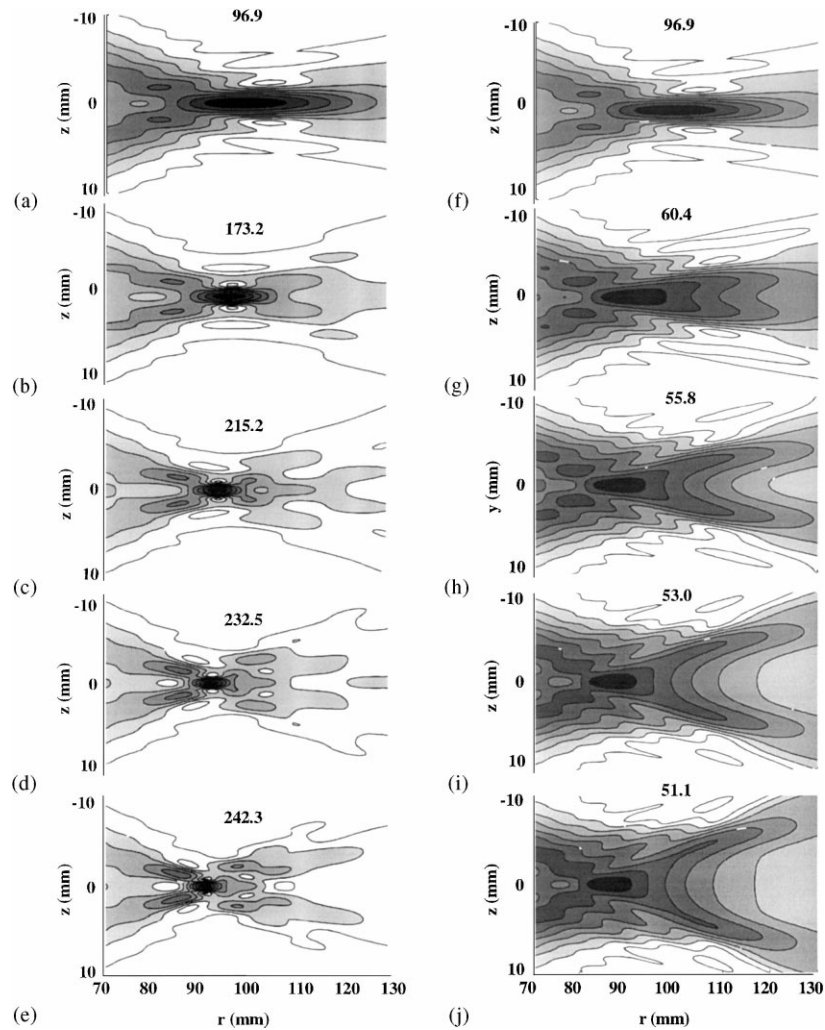


Fig. 5. Pressure field in the treatment region for $\partial c/\partial T = -4 \text{ m/s/}^\circ\text{C}$: (a) $t = 0$, (b) $t = 2.5 \text{ s}$, (c) $t = 5 \text{ s}$, (d) $t = 7.5 \text{ s}$, and (e) $t = 10 \text{ s}$. Pressure field in the treatment region for $\partial c/\partial T = 4 \text{ m/s/}^\circ\text{C}$: (f) $t = 0$, (g) $t = 2.5 \text{ s}$, (h) $t = 5 \text{ s}$, (i) $t = 7.5 \text{ s}$, and (j) $t = 10 \text{ s}$. Each title denotes the maximum value of the acoustic intensity in W/cm^2 .

Fig. 5 represents the time-evolution of the pressure field during the 10 s insonification, for the two cases of a self-focusing and a self-defocusing medium. The time evolution of the pressure field obtained at $t = 10 \text{ s}$ clearly shows the self-focusing or self-defocusing of the acoustic field. If $\partial c/\partial T < 0$, the intensity increases dramatically at the focus, which means that the acoustic field is self-focused, whereas if $\partial c/\partial T > 0$, the intensity decreases which corresponds to a self-defocused effect. In both cases, the focal zone is shifted toward the array up to 10 mm, which corresponds to a ten-wavelength distance. Fig. 6 shows the resulting temperature distributions in the treatment volume at the end of the 10 s insonification.

Two important points are to be highlighted: first, because of the self-focusing and self-defocusing effects, the temperature reached for $\partial c/\partial T < 0$ is much larger than the temperature obtained for $\partial c/\partial T > 0$. Second, the focal shift due to heat-induced acoustic refraction leads to an incorrect estimation of the temperature expected at $r = 100 \text{ mm}$ if the acoustic–heat coupling is neglected. In fact, the focus has moved out of the initial focal plane whatever the sign of $\partial c/\partial T$. This means that the damage done by heat in the zone of interest may not occur at the

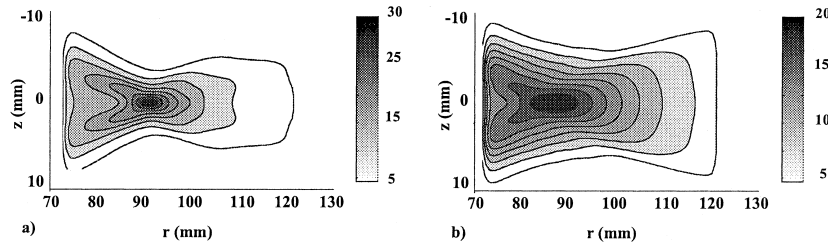


Fig. 6. Temperature elevation (in K) in the treatment volume after 10 s: (a) $\partial c/\partial T = -4 \text{ m/s/}^\circ\text{C}$ and (b) $\partial c/\partial T = 4 \text{ m/s/}^\circ\text{C}$.

desired point. Fig. 6 shows, for example, that the highest temperature elevation after 10 s is located around 90 mm, which is 10 mm away from the initial focal point.

We are now concerned with adaptively keeping the acoustic focus at the desired position as the heating modifies the sound speed. The heat-induced acoustic refraction depends dramatically on the spatial distribution of the acoustic energy in the medium. The larger the focal spot, the larger the zone heated by the acoustic beam and the stronger the acoustic refraction. One solution to maintain the focus at the desired point is to concentrate the acoustic energy around the initial focal spot. To achieve this, we use two arrays focused temporally and spatially at this point: we expect a constructive interference of the acoustic field at the focus and, on the average, a destructive interference everywhere else, which will reduce the focal size around the focal point.

The key problem then is to appropriately phase-delay the two arrays to achieve a constructive summation at the focus. One solution is to take advantage of phase-conjugation invariance properties [14]. Indeed, phase-conjugation invariance ensures that a phase-conjugated field will focus back to its acoustical source regardless of the heterogeneity of the medium and the location of the phase-conjugated mirrors. However, it is generally not practical to place a source at the desired focus before the treatment. To get around this problem, we propose a two-stage procedure based on phase conjugation principles. The first stage is an in vitro computation stage: we model the medium as close as possible to the experimental one. Then we place an acoustic source at the desired focal point and record on the two arrays the incident field, which will focus back to the source after phase conjugation. In the second stage, we use these two phase-conjugated vectors as the source of the two arrays during the in vivo hyperthermia treatment.

Fig. 7 shows an example with two arrays facing each other on each side of the treatment volume. For the same energy at the focus, note that the focal spot is dramatically different from the one obtained with a single array as

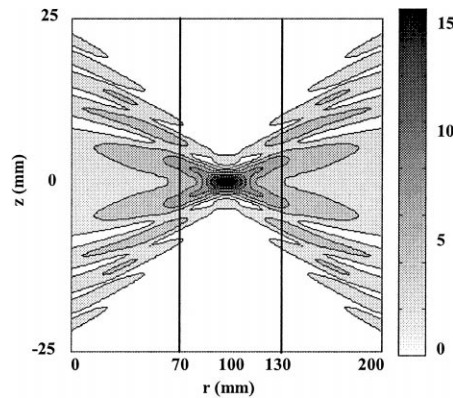


Fig. 7. Acoustic focusing in an absorbing medium using two arrays at $r = 0$ and $r = 200$ mm. Thick solid lines delimit the treatment volume and gray level denotes the pressure in atm. The intensity at the focal point is 97 W/cm^2 .

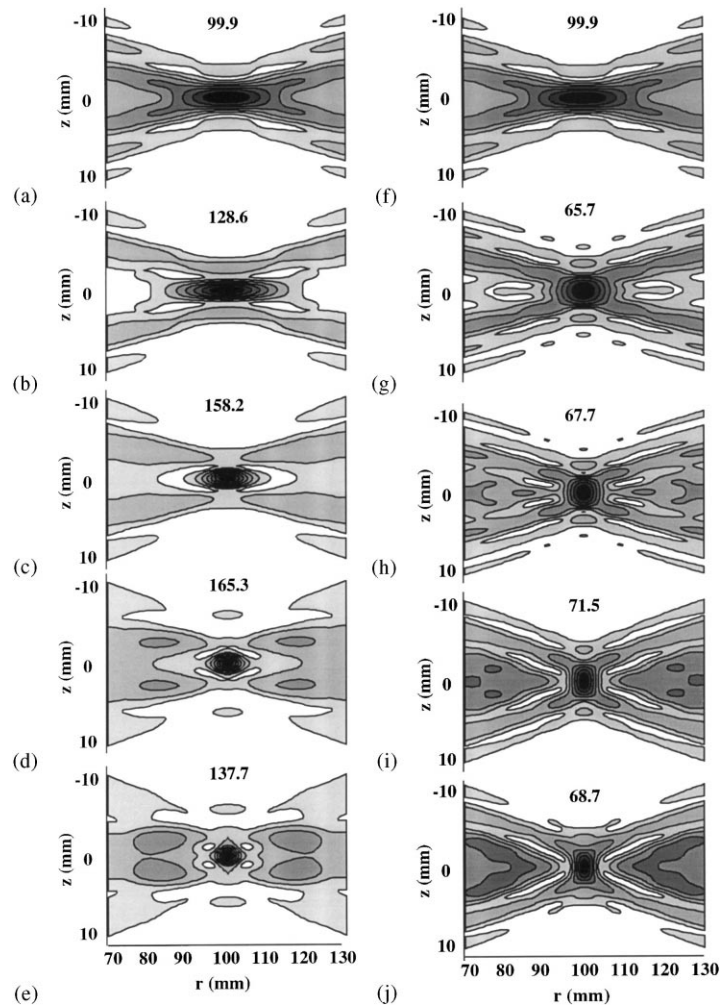


Fig. 8. Pressure field obtained using two arrays in the treatment region for $\partial c/\partial T = -4 \text{ m/s/}^\circ\text{C}$: (a) $t = 0$, (b) $t = 2.5 \text{ s}$, (c) $t = 5 \text{ s}$, (d) $t = 7.5 \text{ s}$, and (e) $t = 10 \text{ s}$. Pressure field in the treatment region for $\partial c/\partial T = 4 \text{ m/s/}^\circ\text{C}$: (f) $t = 0$, (g) $t = 2.5 \text{ s}$, (h) $t = 5 \text{ s}$, (i) $t = 7.5 \text{ s}$, and (j) $t = 10 \text{ s}$. Each title denotes the maximum value of the acoustic intensity in W/cm^2 .

shown in Fig. 3. Following the same format used in Fig. 5, Fig. 8 represents the time evolution of the pressure field during the two-array hyperthermia treatment. The field remains in focus during the entire treatment both for a self-focusing and a self-defocusing medium. Finally, Fig. 9 shows the temperature distribution obtained at the end of the two-array treatment. In comparison with Fig. 6, we see that the field is still in focus at the desired focal point for the same temperature elevation.

The advantage of this two-array treatment is the ability to burn cells accurately. The principal limitation is that the quality of the treatment may depend dramatically on the quality of the numerical phase conjugation experiment made in the first stage. In the future, we will carefully study the consequences of mismatch induced by an incorrect knowledge of the medium. For example, we must investigate what happens during the treatment if the experimental value of the attenuation is not equal to the value used for the numerical experiment.

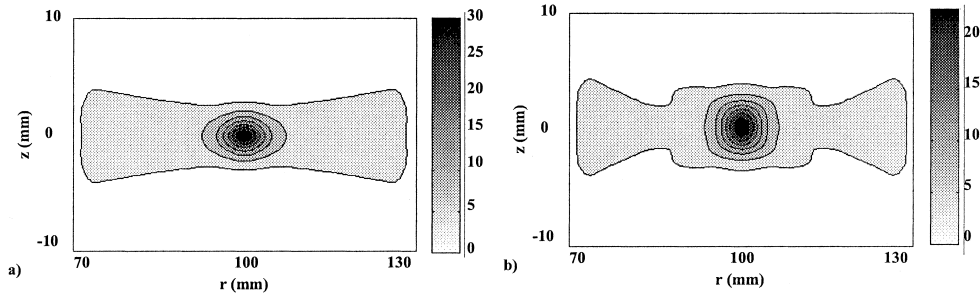


Fig. 9. Temperature elevation (in K) in the treatment volume using two arrays after 10 s: (a) $\partial c/\partial T = -4 \text{ m/s/}^\circ\text{C}$ and (b) $\partial c/\partial T = 4 \text{ m/s/}^\circ\text{C}$.

4. Focal translation by frequency shift in a time-reversal mirror

In this section, we are interested in the focus of the acoustic field on a short timescale around a probe source for an application to acoustic imaging in medical ultrasound.

A time-reversal mirror (TRM, or a phase conjugate array) refocuses an incident acoustic field back to the original position of a probe source (PS) or a scatterer regardless of the complexity of the medium [5]. Recently a variable focal range TRM that works in a waveguide geometry has been developed theoretically [15] and confirmed experimentally in the ocean [16]. The technique involves retransmitting the received data at a shifted frequency according to the desired change in focal range. The formula that governs this shift is

$$\frac{\Delta\omega}{\omega} = \beta \left(\frac{\Delta R}{R} \right), \tag{7}$$

where $\Delta\omega$ is the frequency shift and ΔR is the associated range shift. The acoustic invariant β is determined by the properties of the medium and is approximately equal to 1 for a large class of acoustic waveguides.

In this paper, we extend the idea of frequency shift to the free space problem. In particular, for variable range focusing, the prescribed frequency shift is the same for all elements of the array such that $\beta = 1$ in Eq. (7). On the other hand, for transverse focal shifts, the frequency shift varies with element location in the array as will be described shortly.

Numerical simulations are carried out in two dimensions for two different scenarios. First, we show the proposed shift algorithm with a phase conjugation in a homogeneous medium and compare the results with those from a conventional steering technique. Second, we apply the proposed algorithm to an inhomogeneous medium comprised of two homogeneous media with a rough random interface between them equivalent to a phase screen or an aberrating layer. As shown in Fig. 10, consider a 61-element linear array at zero range with an element spacing of 0.5 mm

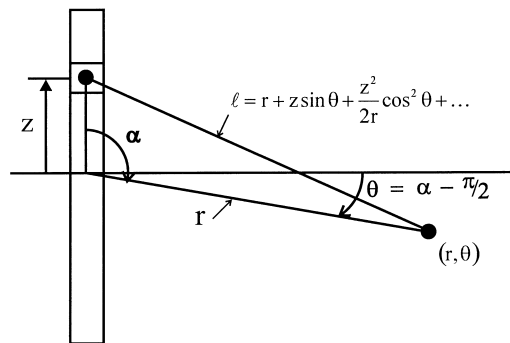


Fig. 10. Spherical coordinate system, and linear array analysis.

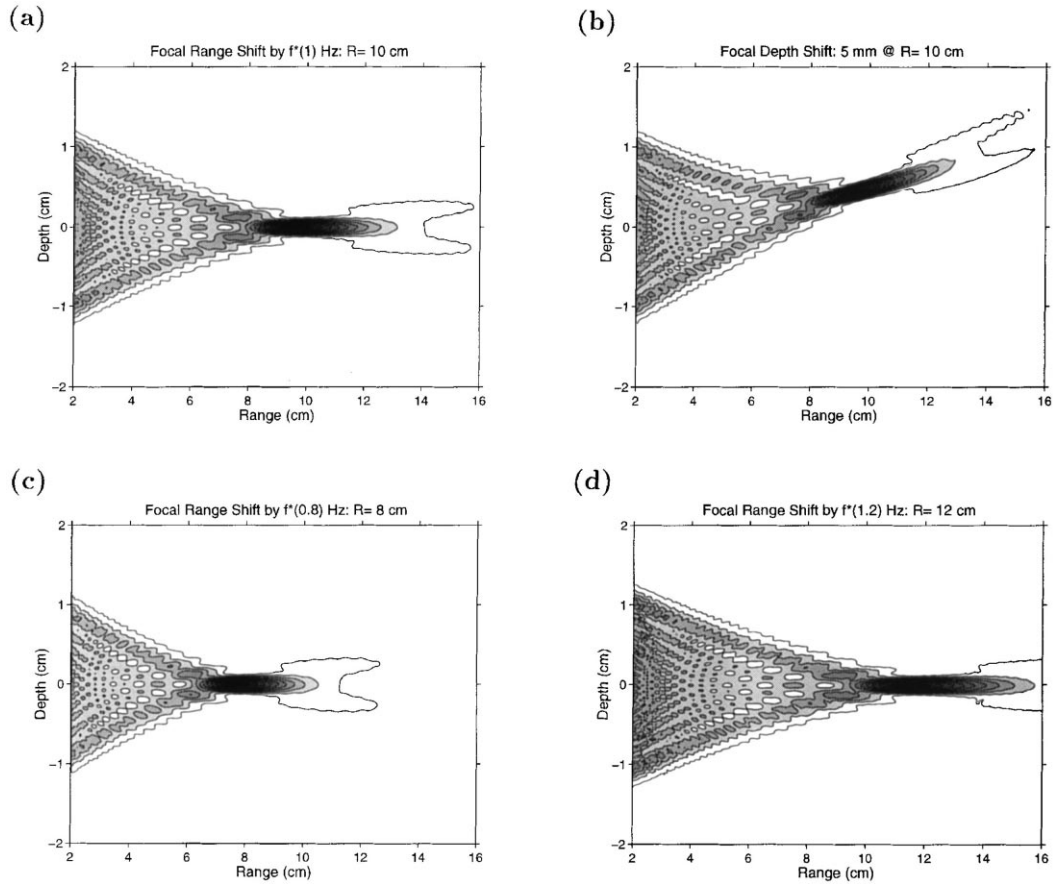


Fig. 11. Focal translation using frequency shift in uniform free space. The original probe source (PS) is located at $R = 10$ cm range from the linear array. (a) Focus at the original PS without frequency shift ($f_0 = 3$ MHz). (b) Moving the focal spot upward by $d = 5$ mm with variable frequency shift along the array ($\Delta f(z) = zdf_0/R^2$). (c) Focus at $R = 8$ cm with a shifted frequency $f = 0.8f_0$. (d) Focus at $R = 12$ cm with a shifted frequency $f = 1.2f_0$. Note that the depth resolution remains the same while the range resolution changes linearly with range.

($L = 30$ mm) which corresponds to one wavelength at 3 MHz carrier frequency with a sound speed of 1500 m/s. The original probe source (PS) is placed at 100 mm range and zero depth. The conventional steering technique is implemented by compensating the phase delay of each element along the array to the intended focal spot in a homogeneous medium. The acoustic field is computed by a wide-angle parabolic equation model developed by Collins [8].

4.1. Focal translation in uniform free space

Fig. 11 shows that the focal spot can be moved in any direction by an appropriate frequency shift. The results from the conventional steering method are also shown in Fig. 12 for comparison. Note that the focused field or the ambiguity function in range and depth is plotted on a linear scale after normalization.

Several important observations can be made. Fig. 11(a) shows that phase conjugation refocuses an incident acoustic field back to the original position of the PS; this is exactly same as Fig. 12(a) by a conventional approach for two reasons. First, the acoustic environment is perfectly specified for the conventional method. Second, the conventional method corresponds to phase conjugation with a virtual PS at the intended focal spot without frequency shift.

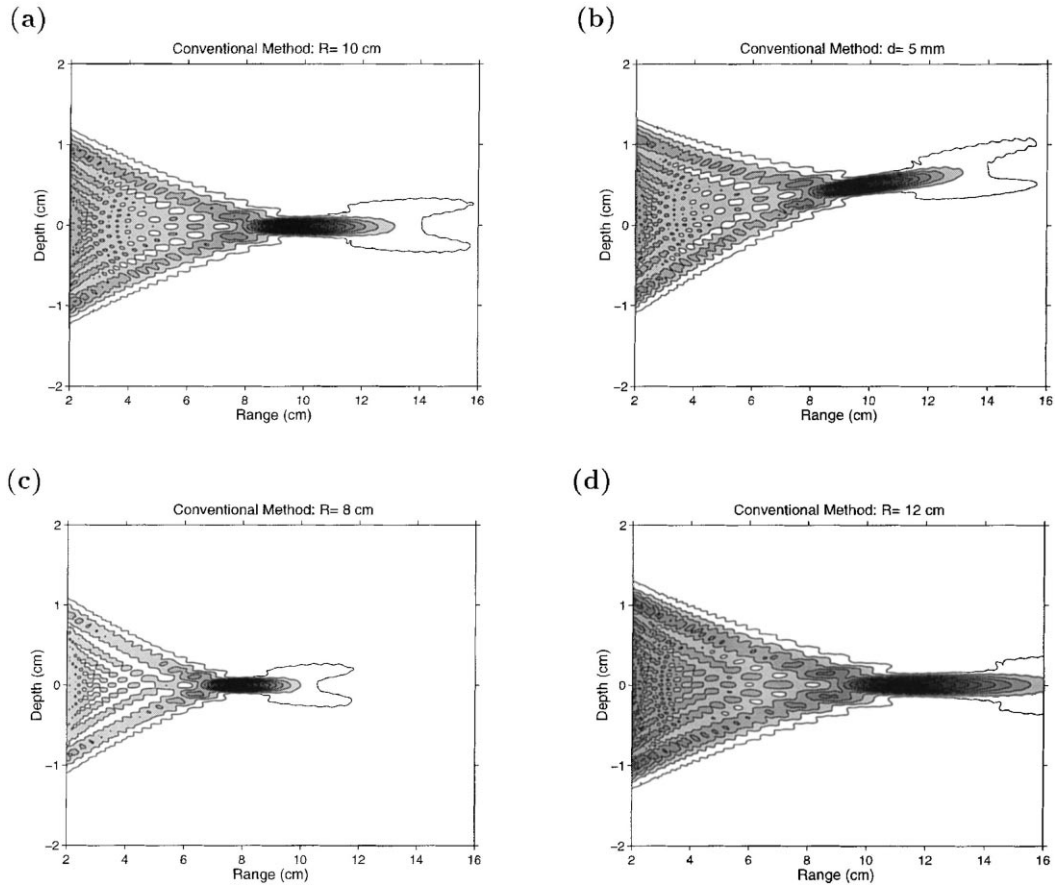


Fig. 12. Focusing at various locations using conventional phase steering as compared to Fig. 11. (a) $R = 10$ cm, $d = 0$ mm, (b) $R = 10$ cm, $d = 5$ mm, (c) $R = 8$ cm, $d = 0$ mm, and (d) $R = 12$ cm, $d = 0$ mm. Note that the depth resolution increases linearly with range while the range resolution changes quadratically with range.

Fig. 11(c) and (d) shows the results of applying a constant frequency shift to all elements of the array prior to retransmission by a factor of 0.8 (2.4 MHz) and 1.2 (3.6 MHz), respectively. As expected, the focal range is now moved to 8 and 12 cm, respectively. Corresponding results by the conventional method are displayed in Fig. 12(c) and (d). It is interesting to note, however, that the resolution in range differs in the two methods.

In classical optics, the resolution in range and depth is determined by the Rayleigh limit:

$$\Delta R = \lambda \left(\frac{R}{L} \right)^2, \quad \Delta Z = \lambda \left(\frac{R}{L} \right). \tag{8}$$

Given the aperture of the array L and λ , the range and depth resolution in the conventional method is then proportional to R^2 and R , respectively. However, for variable range focusing with frequency shift, the range resolution is proportional to R and not quadratic because λ changes inversely proportional to the frequency as well. On the other hand, the depth resolution remains the same due to the opposite effect of R and λ with respect to frequency whereas the depth resolution increases with range in the conventional method as can be observed in Fig. 12(c) and (d).

In order to move the focal spot transversely, an element-dependent frequency shift must be applied to the array element such that

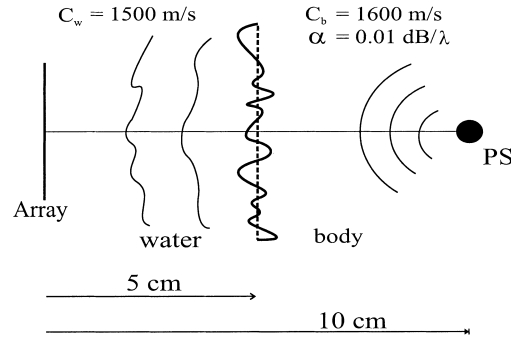


Fig. 13. A schematic of phase conjugation through an inhomogeneous medium. A probe source emits a spherical wave pulse that is received by a linear array after passing through a rough interface between the water and the human body with a Gaussian roughness spectrum defined in Eq. (10). The sound speed and attenuation coefficient of the body are assumed 1600 m/s and 0.01 dB/ λ , respectively.

$$\frac{\Delta\omega}{\omega} = \frac{zd}{R^2}, \quad (9)$$

where z is the element location in the array and d is the desired focal depth (positive in upward direction). Fig. 11(b) shows the results for $d = 10\lambda$ (5 mm) where the maximum frequency shift becomes 22.5 kHz on the edge elements of the array as compared to the conventional steering method result in Fig. 12(b).

In this section, time-reversal steering using frequency shift has been explored along with a conventional steering method in uniform space. It appears that there are no obvious advantages of the proposed method over the conventional method other than different resolutions in range and depth. That is because the medium, which is completely known and homogeneous in uniform free space, permits straightforward implementation of the conventional method. In the next section, we apply the proposed method to an inhomogeneous medium to illustrate the efficiency of time-reversal approach with a frequency shift.

4.2. Focusing through a phase screen

For practical applications to diagnostic imaging systems, consider an inhomogeneous medium consisting of two homogeneous media, water and human body, with a rough interface as shown in Fig. 13. The rough surface is positioned halfway between the PS and the array, i.e., 50 mm away from the PS inside the body. The actual propagation velocity through a body varies from 1440 m/s in fat to 1600 m/s in muscle and the acoustic attenuation/absorption coefficients of most soft tissues range between 5 and 10 Np/m/MHz, or approximately 15 or 30 Np/m at 3 MHz [19]. In our simulations a human body is treated as a homogeneous medium with a sound speed of 1600 m/s and an absorption coefficient of 0.1 dB/ λ . The rough surface is one-dimensional with a Gaussian roughness spectrum:

$$P(k_z) = \sigma^2 \sqrt{2\pi} L_c \exp(-k_z^2 L_c^2 / 2), \quad (10)$$

where L_c is the roughness correlation length and σ is the root-mean-square roughness. For propagation wave vectors k_z parallel to the vertical z -axis, this surface will produce no out-of-plane scattering. For the conventional method, the inhomogeneous medium is taken as a uniform medium with a sound speed either 1500 or 1600 m/s since we assume we have no detailed knowledge of the roughness that can be utilized.

Fig. 14 shows two sets of focal translation results for different scattering strengths: (a)–(d) when $L_c = 5\lambda$ and $\sigma = \lambda$, and (e)–(h) when $L_c = \lambda$ and $\sigma = 2\lambda$. Fig. 14(a), (b) and (d) shows the focal shifts in range with a constant frequency shift by factors of 0.8, 1.0 (no shift) and 1.2, respectively, while Fig. 14(c) displays the focal shift in depth (5 mm) with element-dependent frequency shift. Note that (a)–(d) are very similar to those obtained in uniform free space (see Fig. 11). In this example, the difference in the acoustic medium between the water and the body is not

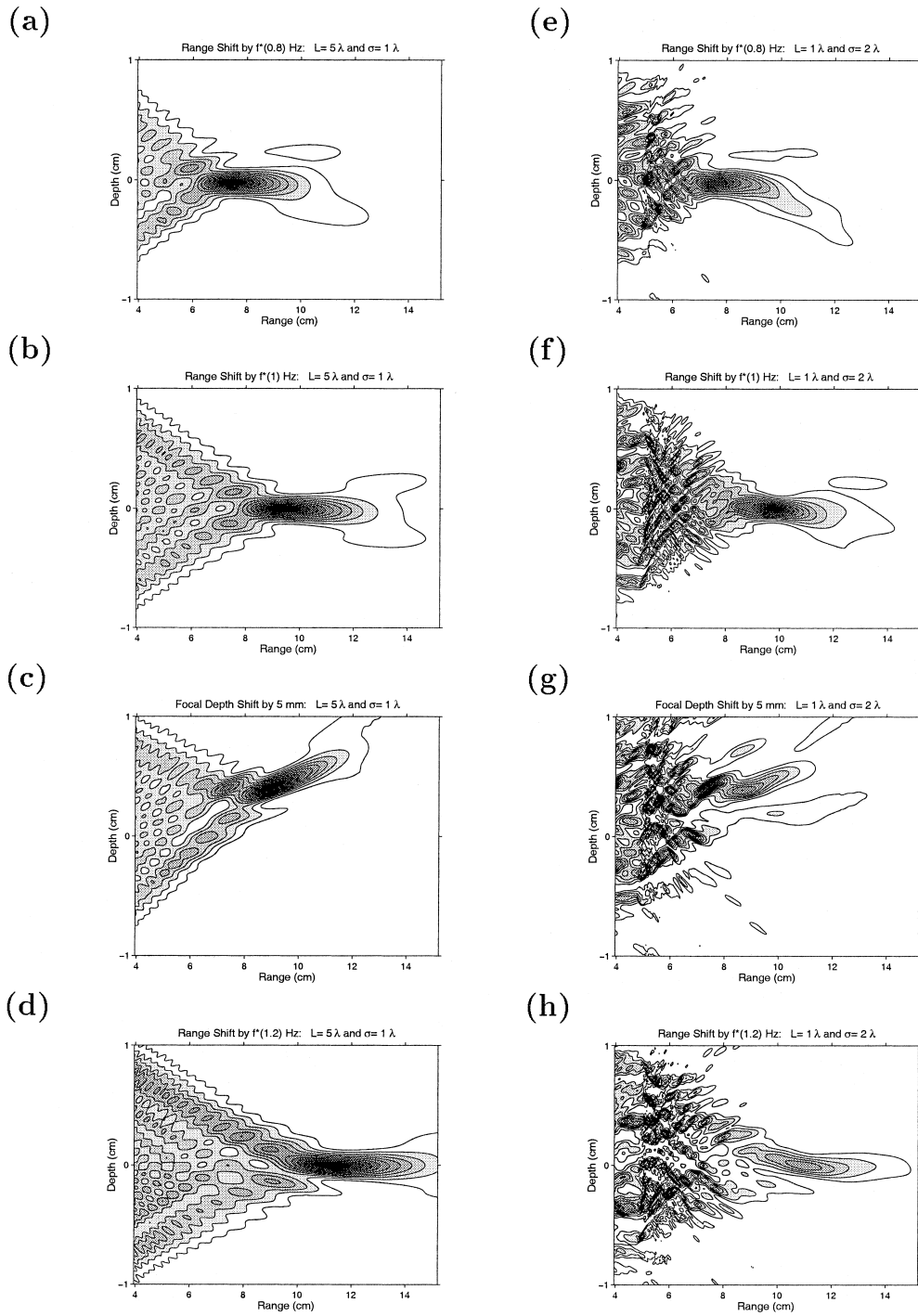


Fig. 14. Focal translation using frequency shift in an inhomogeneous medium for two different rough surfaces at $R = 5$ cm. When $L_c = 5\lambda$ and $\sigma = \lambda$: (a) $f = 0.8f_0$ and $R = 8$ cm, (b) $f = f_0$ and $R = 10$ cm, (c) $\Delta f(z) = zdf_0/R^2$, $R = 10$ cm and $d = 5$ mm, and (d) $f = 1.2f_0$ and $R = 12$ cm. (e)–(h): same as (a)–(d) except that $L_c = \lambda$ and $\sigma = 2\lambda$.

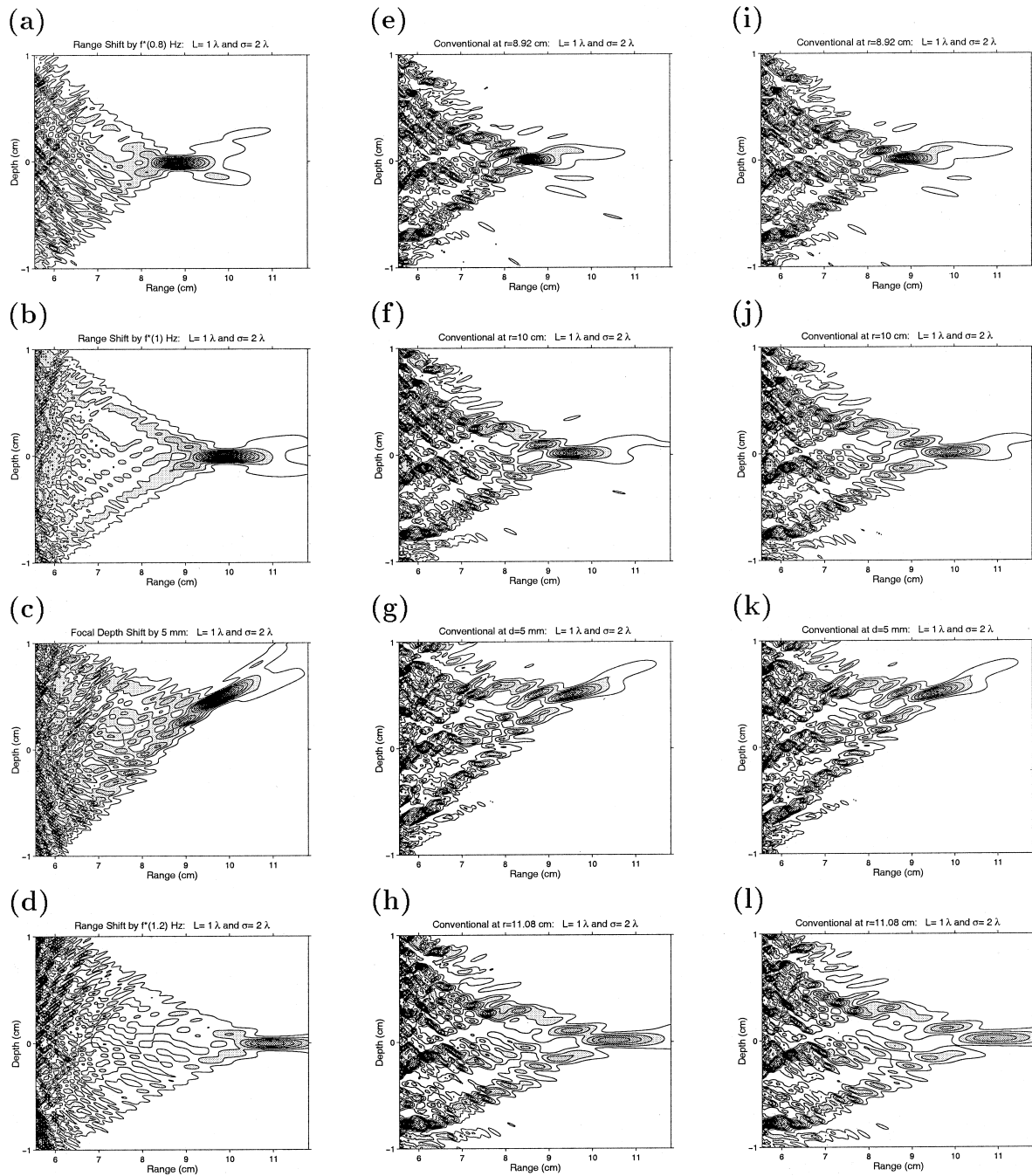


Fig. 15. Comparison between focal translation using frequency shift and a conventional steering assuming a homogeneous medium. The linear array is now positioned at $R = 4$ cm, closer to the phase screen at $R = 5$ cm. Since the distance between the PS and array is 6 cm, 20% shift in frequency results in only 1.2 cm shift in range. Focal translation using frequency shift: (a) $f = 0.8 f_0$ and $R = 8.8$ cm, (b) $f = f_0$ and $R = 10$ cm, (c) $\Delta f(z) = zdf_0/R^2$, $R = 10$ cm and $d = 5$ mm, and (d) $f = 1.2 f_0$ and $R = 11.2$ cm. (e)–(h): conventional steering with a homogeneous sound speed of 1500 m/s. (i)–(l): conventional steering with a homogeneous sound speed of 1600 m/s.

that significant resulting in weak scattering at the rough interface with $L_c = 5\lambda$ and $\sigma = \lambda$, which still allows us to use the proposed frequency shift approach.

For greater roughness when $L_c = \lambda$ and $\sigma = 2\lambda$, however, the frequency shift method breaks down as shown in Fig. 14(e)–(h) except (f) which demonstrates that phase conjugation always refocuses the received field back to the original PS regardless of the complexity of the medium. The difficulty of focal translation in this case arises from the fact that the idea of frequency shift is derived in a homogeneous free space [17].

It is shown in [18] that amplitude and shape distortion develops as the wavefront continues to propagate in a uniform medium passing through the aberrating medium which causes only phase shift (or time delay). The numerical back-propagation of the received field to the aberrating medium would reduce the wavefront distortion, which in turn allows us to apply either the conventional approach or the frequency shift idea for focal translation. In other words, the effect of a phase aberrator on phase conjugation with frequency shift can be minimized by placing an array as close as possible to the aberrator.

To exploit this idea, let us move the array at the origin to $R = 4.6$ cm, closer to the interface at $R = 5$ cm when $L_c = \lambda$ and $\sigma = 2\lambda$. Fig. 15(a)–(d) shows that focal translation with frequency shift can be achieved in the presence of a strong aberrator as long as the array is close to the aberrator. Note that the distance between the array and the PS is now 5.4 cm, not 10 cm so that 20% frequency shift induces only 1.08 cm in range. The increase in attenuation with higher frequency and longer propagation distance also causes a weaker mainlobe around the intended focal spot in Fig. 15(d). In comparison, Fig. 15(e)–(h) and (i)–(l) shows results from the conventional steering method assuming a homogeneous sound speed 1500 m/s and 1600 m/s, respectively. Note that the group of (i)–(l) yields more accurate results in their focal positions than (e)–(h) since the propagation medium is mainly a human body with a sound speed of 1600 m/s. It appears that the conventional method also produces reasonable focal shifts, but certainly not as good as phase conjugation with frequency shift as shown in Figs. 15(a)–(d). It should be mentioned again that phase conjugation is an environmentally self-adaptive process that does not require environmental information, whereas our conventional approach assumes a homogeneous medium with a sound speed to be estimated.

5. Conclusions

We have shown numerically that in a medium with attenuation, heat induced by acoustic focusing leads to refraction of acoustic waves and disturbs the focus. The effect observed at the focus is either a self-focusing or a self-defocusing of the acoustic beam depending on the sign of dc/dT in the medium. A procedure is proposed to maintain focus in the zone of interest using two arrays and phase-conjugation invariance properties. For application to medical imaging, an algorithm is proposed that can shift the focal spot of a linear array both transversely and horizontally in free space. For variable range focusing, the frequency shift is the same for all elements of the array whereas for transverse focal shifts, the frequency shift varies linearly along the array. Simulations demonstrate the efficiency of this approach over the conventional method in an inhomogeneous medium with a strong aberrator in that no knowledge of the medium properties is required.

References

- [1] M.A. Leontovich, V.A. Fock, Solution of the problem of propagation of electromagnetic waves along the earth's surface by the method of parabolic equation, *J. Exp. Theor. Phys.* 16 (1946) 557–573.
- [2] F.D. Tappert, The parabolic approximation method, in: J.B. Keller, J.S. Papadakis (Eds.), *Wave Propagation and Underwater Acoustics*, Lecture Notes in Physics, vol. 70, Springer, New York, 1977, pp. 224–280.
- [3] J.F. Claerbout, *Fundamentals of Geophysical Data Processing*, Blackwell, Oxford, 1985, pp. 194–207.
- [4] C. Le Floch, M. Tanter, M. Fink, Self-defocusing in ultrasonic hyperthermia: experiment and simulation, *Appl. Phys. Lett.* 74 (1999) 3062–3064.
- [5] M. Fink, Time-reversed acoustics, *Phys. Today* 50 (1997) 34–40.
- [6] M.D. Collins, R.J. Cederberg, D.B. King, S.A. Chin-Bing, Comparison of algorithms for solving parabolic wave equations, *J. Acoust. Soc. Am.* 100 (1996) 178–182.

- [7] M.D. Collins, E.K. Westwood, A higher-order energy–energy conserving parabolic equation for range-dependent ocean depth, sound speed, and density, *J. Acoust. Soc. Am.* 89 (1991) 1068–1075.
- [8] M.D. Collins, Generalization of the split-step Padé solution, *J. Acoust. Soc. Am.* 93 (1993) 382–385.
- [9] H.H. Pennes, Analysis of tissue and arterial blood temperatures in the resting human forearm, *J. Appl. Physiol.* 1 (1948) 93–122.
- [10] M. Kolios, M. Sherar, J. Junt, Modeling temperature gradients near large vessels in perfused tissues, in: M. Ebadian, P. Oosthuizen (Eds.), *Fundamentals of Biomedical Heat Transfer*, ASME, New York, 1994.
- [11] R.J. McGough, M.L. Kessler, E.S. Ebbini, C.A. Cain, Treatment planning for hyperthermia with ultrasound phased arrays, *IEEE Trans. Ultrason. Ferroelect. Freq. Contr.* 43 (1996) 1074–1084.
- [12] C.A. Damianou, N.T. Sanghvi, F.J. Fry, R. Maass-Moreno, Dependence of ultrasonic attenuation and absorption in dog soft tissues on temperature and thermal dose, *J. Acoust. Soc. Am.* 102 (1993) 628–634.
- [13] V.G. Andreev, A.A. Karabutov, O.V. Rudenko, O.A. Sapozhnikov, Observation of self-focusing of sound, *JETP Lett.* 9 (1985) 466–469.
- [14] P. Roux, M.B. Porter, H.C. Song, W.A. Kuperman, Hyperthermia therapy using phase conjugation, in: *Proceedings of the 24th International Symposium on Acoustical Imaging*, Santa Barbara, CA, 1998.
- [15] H.C. Song, W.A. Kuperman, W.H. Hodgkiss, A time-reversal mirror with variable range focusing, *J. Acoust. Soc. Am.* 103 (1998) 3234–3240.
- [16] W.H. Hodgkiss, H.C. Song, W.A. Kuperman, T. Akal, C. Ferla, D. Jackson, A long-range and variable focus phase-conjugation experiment in shallow water, *J. Acoust. Soc. Am.* 105 (1999) 1597–1604.
- [17] H.C. Song, P. Roux, W.A. Kuperman, Focal translation by frequency shift in free space, *IEEE Trans. Ultrason. Ferroelect. Freq. Contr.*, accepted.
- [18] C. Dorme, M. Fink, Ultrasonic beam steering through inhomogeneous layers with a time-reversal mirror, *IEEE Trans. Ultrason. Ferroelect. Freq. Contr.* 43 (1996) 167–175.
- [19] S.A. Goss, R.L. Johnston, F. Dunn, Comprehensive compilation of empirical ultrasonic properties of mammalian tissues, *J. Acoust. Soc. Am.* 64 (1997) 423–457.